analytical chemistry

pubs.acs.org/ac Article

# Complementary Nanoparticle Characterization by Resistive-Pulse Sensing, Electron Microscopy, and Charge Detection Mass Spectrometry

Lohra M. Miller,[†] Tanner W. Young,[†] Yi Wang, Benjamin E. Draper, Xingchen Ye, Stephen C. Jacobson,* and Martin F. Jarrold*

Cite This: https://doi.org/10.1021/acs.analchem.4c02901 Read Online



**ABSTRACT:** Nanotechnology has provided novel modalities for the delivery of therapeutic and diagnostic agents. In particular, nanoparticles (NPs) can be engineered at a low cost for drug loading and delivery. For example, silica NPs have proven useful as a controlled release platform for anti-inflammatory drugs. Despite the wide-ranging potential applications for NPs, robust characterization across all size ranges remains elusive. Electron microscopy (EM) is the conventional tool for measuring NP diameters. However, imitations in throughput and the inability to provide comprehensive information on physical properties, such as mass and density, without underlying assumptions, hinder a complete analysis. In addition, assessing sample heterogeneity, aggregation, or coalescence in solution by traditional EM analysis is not possible. Resistive-pulse sensing (RPS) provides a high throughput, solution-phase method for characterizing particle heterogeneity based on volume. Complementing these methods, charge detection mass spectrometry (CD-MS), a single particle technique, provides accurate mass information for heterogeneous samples including NPs. By combining EM, RPS and CD-MS, accurate volume, mass, and densities were obtained for silica NPs of various sizes. The results show that the density for 20 nm silica NPs is close to the density of fused silica (2.2 g/cm$^3$). Larger silica NPs were found to have densities that were either smaller or larger, while also falling outside the range of densities usually found for silica colloids and NPs (1.9−2.3 g/cm$^3$). Lower densities are attributed to pores (i.e., porous particles). For one sample, the mass distribution showed two components attributed to two populations of particles in the sample with different densities. The synergistic combination of EM, RPS, and CD-MS measurements outlined here for NP samples, allows much more extensive information to be obtained than from any of the techniques alone.

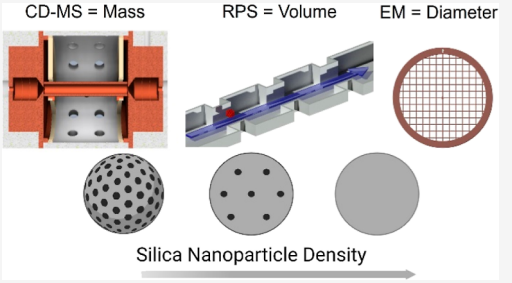


## INTRODUCTION

Nanoparticles (NPs), 1−100 nm in diameter, have a growing impact in healthcare as they provide better delivery vehicles for therapeutic and diagnostic agents. There are currently over 30 NP therapeutics in clinical use, in addition to other NP agents in the preclinical and clinical phases of drug development.[1] A recent breakthrough was the use of lipid-nanoparticles as a drug delivery vehicle for the SARS-CoV-2 mRNA vaccine.[2] NPs reduce degradation by host enzymes, offer controlled drug release, and have the ability to be functionalized with small molecules for precision targeting of the optimum site for release.[3−5] Silica NPs perform similar functions in drug delivery with an advantage in structure tunability and established strategies for numerous surface modifications.[6−8] One example of silica as an effective drug delivery system is the slow, controlled release of an anti-inflammatory drug such as ibuprofen.[9,10]

Silicon dioxide or silica is a model metal-oxide system as it is biocompatible, has low toxicity, and is stable both chemically and thermally. Silica has shown unique advantages in the field of nanomedicine, as seen in the engineering of silica particles to load and deliver drugs to cancer cells and to deliver gene therapies to treat genetic diseases.[11−14] Surface capping agents have been developed that allow applications as diverse as facile transport across the blood−brain barrier and decreased viral transduction.[15,16] Silica has also been modified to a mesoporous form that has had applications in catalytic components, nanodevices for controlled delivery, and nanoscopic reactors and containers.[17−22] Applications of silica NPs have also emerged in the oil and gas industry where drag reduction in porous media has led to enhanced oil recovery and the reduction of water invasion in shale.[23]

Traditional methods to determine the size of NPs include several ensemble averaging methods such as various light

Received: June 5, 2024
Revised: August 9, 2024
Accepted: August 14, 2024

scattering techniques.[24] Dynamic light scattering characterizes particles based on Brownian motion and provides quick sample characterization. However, accurate measurements for particles below ~50 nm can be challenging.[24−26] In addition, ensemble averaging of NPs results in a loss of information regarding the heterogeneity of the sample as infrequent events often are misrepresented.[27] Single-particle characterization techniques are better suited to providing insight into a sample's heterogeneity. With recent advances in nanotechnology applications, the need for analytical tools that provide robust and accurate characterization of NP heterogeneity for various physical properties such as size, mass, and density are of high importance.

Electron microscopy (EM) is a routine analytical tool for single particle size determination for NPs. Transmission electron microscopy (TEM) analysis has allowed for the statistical investigation of a large range of NP sizes, but a critical property that cannot be determined from TEM is an accurate mass or density. The bulk density of fused silica is 2.203 g/mL. However, silica NPs do not necessarily have the same density. Kimoto and colleagues recently showed that silica NPs ranging from 40 to 200 nm had an average density of 1.9 g/mL.[28] Determining how the densities of silica NPs vary depending on the synthetic method can provide insight into physical properties such as packing density, core porosity, and particle deformation; all important characteristics for sample preparation and formulation for future applications.

While TEM can provide insight into particle size distributions, it is not a high-throughput technique, and it provides information in a 2D projection, so volume determinations are qualitative at best. Resistive-pulse sensing (RPS),[29,30] on the other hand, is a volume-based measurement where particle counts of >1000 counts $min^{-1}$ can be achieved.[31] In RPS, the particle volume is determined from the volume of electrolyte displaced as the particle passes through a nanopore. When a particle enters a nanopore, the displaced electrolyte results in a change in current with respect to the baseline current through the pore ($\Delta i/i$) that is proportional to the displaced volume and hence the volume of the analyte. Multiple pores can be placed in series,[32,33] and signal averaging for each particle enhances the overall resolution.[34] As a single particle technique, RPS can provide insight into true heterogeneity of a sample, and this information is determined directly for samples while in solution, providing a method with no possibility for image biasing.

Combining the size and volume information from TEM and RPS, respectively, with an accurate mass measurement yields an accurate density. In general, mass distributions for NPs cannot be measured by conventional mass spectrometry because of the inability to resolve charge states due to the inherent heterogeneity of these samples. However, charge detection mass spectrometry (CD-MS) has been used to measure the mass of NPs greater than 70 nm.[35−37] CD-MS does not require charge state deconvolution as both the mass-to-charge ($m/z$) and charge ($z$) are measured simultaneously for each ion to give a mass distribution for even the most heterogeneous analyte.[38−50] Combining the single particle mass measurement of CD-MS with the particle volume measurements obtained by RPS allows a precise measurement of silica NP density. The results show that the density varies with particle preparation method and size.

## EXPERIMENTAL METHODS

**Silica NPs.** Commercial silica NP samples (nominally 20, 30, and 50 nm diameter) were purchased from nanoComposix. All samples were approximately 5 mg/mL in DI water and diluted 10−100 times with acetic acid solution for electrospray. In addition, silica NPs were synthesized in-house using established protocols detailed elsewhere.[51] Seed particles were prepared by the sequential addition of 54.6 mg of L-arginine (99.5%, Sigma-Aldrich), 41.4 g of water, and 3.13 g TEOS (98%, Acros Organics) into a 125 mL Erlenmeyer flask. The solution was stirred at 500 rpm and held at 60 °C for 24 h.

The seed particles (14.2 ± 1.7 nm in diameter) were then used to prepare the other sizes of silica NPs discussed herein (see Table 1). To synthesize larger particles, 87 mg L-arginine was first mixed with the appropriate amount of water, ethanol, and seed solution. Subsequently, TEOS was injected rapidly while stirring at 500 rpm. The reaction mixture was kept at 60 °C for 24 h. The particles were precipitated by adding twice the volume of acetone, centrifuged at 4000 rpm for 3 min, and redispersed in 20 mL of ethanol. One additional purification was performed by adding 40 mL of acetone, centrifuging at 4000 rpm for 3 min, and then redispersing in water to a concentration of 5 mg/mL. The synthetic details are summarized in Table 1.

**Table 1. Reaction Conditions for Different Sized Silica NPs**

| NP diameter (nm)[a] | seed (mL) | water (g) | ethanol (g) | TEOS (mL) |
|---|---|---|---|---|
| 19.6 ± 1.1 nm | 14.1 | 27.0 | 65.8 | 1.9 |
| 42.5 ± 3.2 nm | 0.96 | 24.5 | 62.9 | 1.3 |
| 72.5 ± 4.0 nm | 0.56 | 24.5 | 62.9 | 2.8 |

[a]Determined by TEM.

**Electron Microscopy.** TEM images were acquired with a JEOL JEM-1400 at an accelerating voltage of 120 kV. TEM grids were prepared by drop-casting a NP dispersion onto a carbon-coated copper grid and allowing the sample to dry in air. Particle size distributions were obtained from statistical analysis of TEM images. Over 200 particles were detected and analyzed with a custom MatLab script (Mathworks, Inc.).

Images of commercial NPs were acquired with a scanning electron microscope (SEM) (Auriga 60 Crossbeam, Carl Zeiss, GbmH) with an acceleration voltage of 2.00 kV. A 0.5 $\mu$L aliquot of particles, suspended in $H_2O$, was drop-cast onto a Cr coated coverslip and dried at 60 °C for 30 min prior to imaging. Over 200 particles were analyzed by measuring their horizontal lengths with ImageJ Micro-Manager 2.0.

**Resistive-Pulse Sensing.** The nanofluidic devices were fabricated as previously described (see Figure S1a).[34,52] The microchannels were etched to a depth of 8 $\mu$m and measured with a stylus-based profiler (KLA Tencor T-7). Nanofabrication was completed with the Auriga 60 Crossbeam. Focused ion beam milling was controlled by a nanopatterning and visualization engine (Fibics, Inc.), and milled structures were imaged with the SEM. All nanochannels and nanopores were milled with a beam current of 50 pA at 30 kV. The nanochannels prior to the first pore and between each pore were milled with a dose of 1.58 nC/$\mu m^2$. The nanopores were milled at 0.45 nC/$\mu m^2$ to a width of 75 nm (20 nm silica), 0.6 nC/$\mu m^2$ to a width of 105 nm (50 nm silica), or 0.7 nC/$\mu m^2$ to a width of 115 nm (70 nm silica) with pore lengths of 600 nm. A nanofilter was placed upstream from the detection region to minimize clogging (see Figure S1b). The nanofilter


https://doi.org/10.1021/acs.analchem.4c02901
Anal. Chem. XXXX, XXX, XXX−XXX

contained five or six parallel nanopores that had the same dimensions as the pores in the detection region. Glass devices were then cleaned, bonded, and annealed.

Prior to running samples, each device was sequentially flushed with $H_2O$, 0.1 M NaOH, and $H_2O$ for 10 min each. Silica NP samples were sonicated for 5 min prior to being loaded onto the microfluidic channels. RPS measurements were recorded in 50 mM HEPES with 1 M NaCl and 0.01% Tween-20 at pH 7.5 with a 1.0 V potential applied from an Axopatch 200B (Molecular Devices, Inc.) at a 100 kHz sampling frequency, a gain of $\alpha = 2$, a head stage amplification of $\beta = 0.1$, and a low-pass filter frequency of 10 kHz. For 50 and 70 nm silica particles, three-pore systems (see Figure S1c) with dimensions of 105 × 120 × 600 nm and 115 × 160 × 600 nm ($W \times D \times L$), respectively, were used to characterize particle distributions. For 20 nm silica particles, a two-pore system with dimensions of 60 × 75 × 600 nm was used. Nanopore depths were confirmed with an atomic force microscope (AFM; MFP-3D, Asylum Research, Inc.). Reducing the sensor to a two-pore system improves the limit of detection when compared to a three-pore system.[34] Measurement times were typically an hour and the resolving power is around 25 for the measurements reported here.

All data were imported into MatLab R2020b, and current pulse amplitude ($\Delta i$), pulse width ($w$), and baseline current ($i$) were extracted from the raw data with a modified version of Open Nanopore 1.4.[53] The pulse amplitudes from each set of pulses was averaged, divided by the baseline current, and multiplied by 100 to report the relative pulse amplitude ($\Delta i/i$) as a percentage. The $T = 3$ and $T = 4$ capsids of hepatitis B virus (HBV)[52] were used as calibration standards for the resistive-pulse measurements. The $T = 3$ and $T = 4$ capsids of HBV have zeta potentials of approximately −10 mV and equivalent diameters of 25 and 28 nm, respectively, when measured in the 50 HEPES with 1 M NaCl at pH 7.5. The ratios of the current pulse amplitudes for $T = 3$ and $T = 4$ capsids are similar for measurements in 50 mM HEPES with 0.4, 0.75, and 1 M NaCl at pH 7.5.

**Charge Detection Mass Spectrometry.** All samples were electrosprayed (using positive mode) with a commercial chip-based nanospray source (Advion Triversa Nanomate) into our updated prototype CD-MS instrument described in detail elsewhere.[42,54] Briefly, ions enter the instrument through a metal capillary where they are desolvated and thermalized in an ion funnel/ion carpet hybrid known as a FUNPET.[36] Ion energies are set upon exiting the RF only hexapole and after a series of ion optics, the ions enter an electrostatic linear ion trap (ELIT) based on the cone trap design.[55] Ions oscillate back and forth passing through a conducting cylinder housed within the ELIT. As trapped ions pass through the cylinder, they induce a charge which is detected by a charge sensitive amplifier. The periodic signal is amplified, digitized, and then analyzed by a series of discrete fast Fourier transforms.[43,50] The frequency of the periodic signal is related to the mass-to-charge ($m/z$) and the magnitude of the signal is related to the charge ($z$). The simultaneous measurements of $m/z$ and $z$ allow for a direct determination of the NPs' mass. Measurements are performed for thousands of ions, and then, the results are binned into a mass histogram. Mass versus charge scatter plots for each sample are given in Supporting Information (Figure S5). The prototype CD-MS instrument used for these studies employs a cone trap. It has a relatively low mass resolving power of 50−100 (depending on the charge and $m/z$). Only single ion trapping events are analyzed with the prototype CD-MS instrument, leading to data acquisition times of around an hour. Much higher mass resolving powers and much shorter measurement times are available on newer CD-MS instrument designs.[56,57]

## RESULTS AND DISCUSSION

**Size and Density of 19 nm Silica NPs.** Sample 1, silica NPs of nominally 19 nm in diameter, synthesized by seeded growth, were analyzed by TEM and CD-MS. For CD-MS, the samples were diluted immediately before electrospray with an electrospray compatible solution (ammonium acetate). Figure 1a shows CD-MS mass measurements for over 3600 silica NPs.

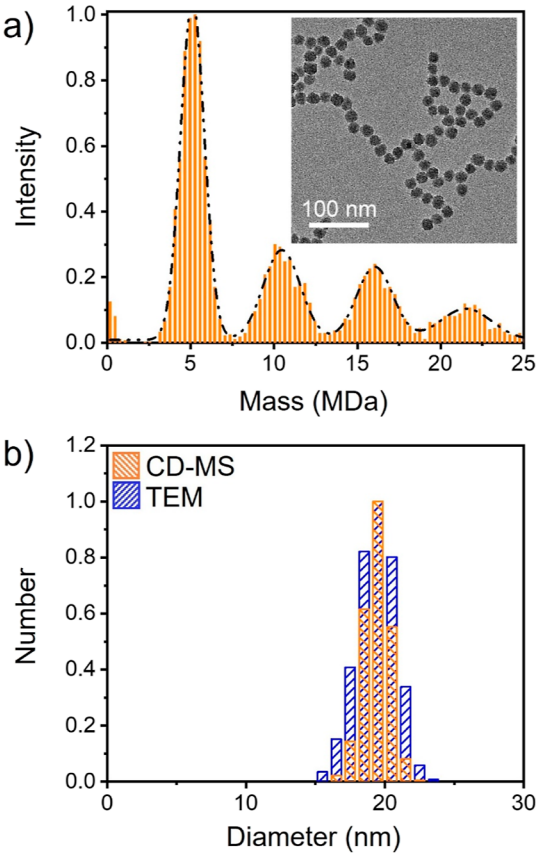


**Figure 1.** Distributions for 19 nm silica NPs prepared by seed mediated growth. (a) CD-MS mass distributions. The dashed-dotted line shows the sum of Gaussians fit to determine the average mass for each component. (b) Diameter distributions determined from the TEM images (blue histogram) and from the mass measurements (orange histogram) with the bulk density (see text). The bin size is 1 nm. The inset in (a) shows portion of a representative TEM image used to determine the diameters. The total numbers of particles analyzed were >3600 for CD-MS and >900 for TEM.

The resultant mass distribution shows four separate populations. Average masses (5.1, 10.5, 16.1, and 21.5 MDa, respectively) were determined by fitting Gaussians to the four peaks. The most abundant peak at 5.1 MDa is attributed to the ∼19 nm silica NPs. The higher mass peaks, separated by an average mass increment of 5.4 MDa, are attributed to aggregates of the ∼19 nm NPs. TEM images showed no evidence that particles had combined to form aggregates during synthesis. The boundaries of the particles are well-defined and there are no "dumbbell" shaped morphologies in


https://doi.org/10.1021/acs.analchem.4c02901
Anal. Chem. XXXX, XXX, XXX−XXX

the TEM images. To explore whether aggregation occurred during sample storage, the samples were gently sonicated for 5 min, and then, the CD-MS spectra were remeasured. Gentle sonication resulted in a noticeable reduction in the higher mass particles (see Figure S2) indicating that the higher mass peaks result mainly from weakly bound aggregates that form during sample storage. Some aggregation could also occur during the electrospray process.

Analysis of over 900 silica particles in the TEM images yielded an average diameter of 19.4 nm with a full width at half-maximum (fwhm) of 3.4 nm. The distribution of particle diameters is shown in Figure 1b as the blue shaded histogram. By combining the mass obtained by CD-MS with the density of the silica NPs, a diameter for each NP can be calculated from

$$d = \left(\frac{6\pi m}{\rho}\right)^{1/3} \quad (1)$$

where $m$ is the particle mass and $\rho$ is the density. Silica colloids or NPs have been reported to have a range in densities from 1.9 to 2.3 g/cm$^3$.[28,51] As a starting point, we used the density of fused silica (2.203 g/cm$^3$). The mass to diameter conversion using eq 1 was performed for each ion in the mass distribution, and then, the results were binned into a histogram of diameters. We only took ions from the lowest mass distribution in Figure 1a. The result is shown in Figure 1b as the orange histogram. The average diameter determined in this way is 19.4 nm, and the fwhm is 2.3 nm. Comparison of the TEM and CD-MS diameter distributions in Figure 1b shows that the centers of the distributions are statistically identical. On the other hand, the width of the distribution determined by TEM is slightly broader than that obtained by CD-MS. The broader distribution from the TEM analysis is probably a result of imprecision introduced by the TEM image analysis (i.e., the difficulty in accurately defining the particle edges) and because the particles are not perfectly spherical. The fact that the distributions are centered on the same diameter indicates that the density of the silica NPs is very close to the density for fused silica (2.203 g/mL) and within the range previously reported for colloidal silica (1.9−2.3 g/cm$^3$).[28,51]

**Analysis of 22 nm Silica NPs by RPS, TEM, and CD-MS.** TEM does not allow high throughput sampling and does not provide direct information about how analytes behave in solution. In addition, TEM provides a 2D projection and most NPs are not perfectly spherical. RPS, on the other hand, can perform high throughput measurements and probes samples directly in solution, providing information about particle interactions in solution during sample analysis as well as providing a more direct volume measurement. As RPS is a single particle detection method, information about sample heterogeneity can also be determined, and as shown here, RPS can also provide information on particle densities when coupled with CD-MS measurement of the mass.

The CD-MS mass distribution measured for sample 2, a ∼22 nm diameter commercial product, is shown in Figure 2a. There are two main components. The lower mass, more abundant peak is attributed to 22 nm silica NPs, and the higher mass peak is assigned to dimers. The 22 nm sample shows less aggregation than the 19 nm sample discussed above (compare Figures 1a and 2a). The dashed-dotted line in Figure 2a shows a Gaussian fit to the two main peaks present in this distribution. The average mass of the main component is 7.5 MDa. The average mass of the peak attributed to the dimer is 14.5 MDa, slightly less than twice the average mass of the monomer. Figure 2b shows the diameter distribution obtained from the CD-MS mass distribution with eq 1 and the bulk density of fused silica. The average diameter for the main component is 22.2 nm, and the fwhm is 3.9 nm. The average diameter given in the certificate of analysis was 22.2 nm (blue line in Figure 2b). The average diameter from the certificate of analysis (obtained from analysis of TEM images for 100 particles) and the average diameter from the CD-MS masses

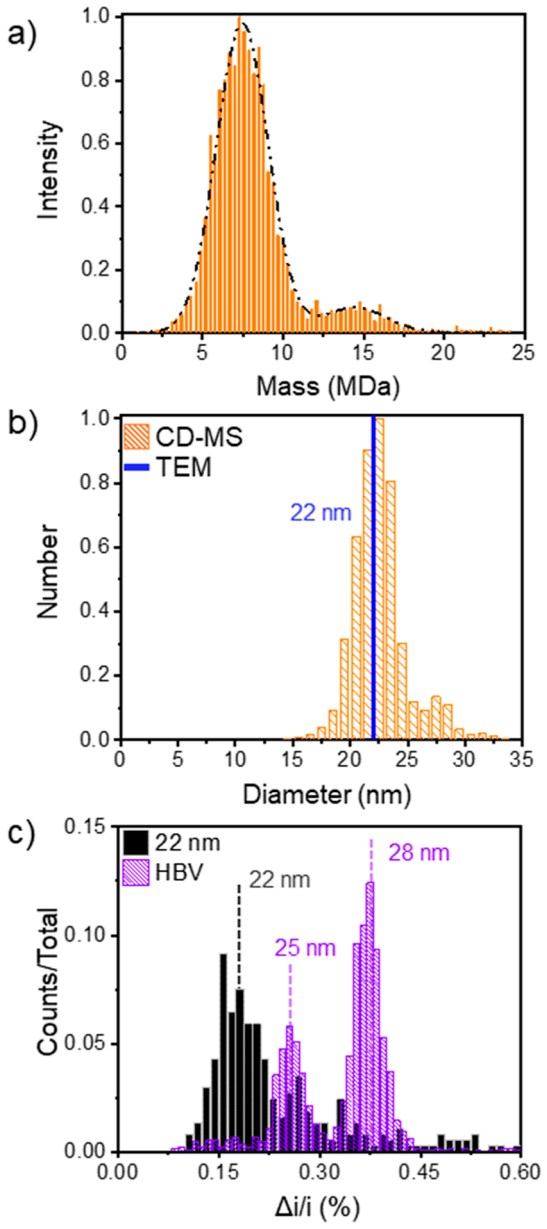


**Figure 2.** Distributions measured for commercial 22 nm silica NPs. (a) CD-MS mass distributions. The dashed-dotted line shows the sum of Gaussians fit to the two main components. (b) Diameter distribution (orange histogram) obtained from the mass distribution in (a) (see text). The bin size is 1 nm. The blue line shows the average diameter from the manufacturers certificate of analysis (determined from TEM measurements). (c) RPS data. Distributions of the 20 nm silica NPs (black) compared to HBV standard (overlaid purple). Total counts were ∼300 and 1700 for RPS of silica and the standard, respectively, and >4000 for CD-MS.


https://doi.org/10.1021/acs.analchem.4c02901
Anal. Chem. XXXX, XXX, XXX−XXX

with the density of bulk fused silica are in close agreement indicating that the density of the silica NPs is close to the density of fused silica and within the range previously reported for colloidal silica.

In RPS, particles are detected from the volume of the electrolyte displaced by the particle. When the particle is inside a nanopore, the displaced electrolyte causes a reduction in the current traveling through the nanopore. The reduction is proportional to the volume of the particle and is represented by the relative pulse amplitude, $\Delta i/i$, where $i$ is baseline current and $\Delta i$ is the decrease in the current as the particle passes through the nanopore. The transmission of a particle through the nanopore leads to a pulse in $\Delta i/i$, or series of pulses for devices with more than one nanopore in series (see Figure S1c). RPS data for sample 2 are shown in Figure 2c. The black distribution shows particle counts plotted against $\Delta i/i$. With standards of known volume, the $\Delta i/i$ values measured for the silica particles can be translated into volumes from which the average diameter can then be determined for each particle. The standard used in this case is HBV capsids. The truncated HBV capsid protein Cp149 assembles to give icosahedral $T = 3$ capsids with 180 capsid proteins (26 nm) and $T = 4$ capsids with 240 capsid proteins (29 nm).[58,59] The RPS data measured for the HBV standard is shown as the overlaid purple distribution in Figure 2c. The equivalent diameters of the $T = 3$ and $T = 4$ capsids measured with RPS are 25 and 28 nm, respectively, which correspond well with the diameters measured by EM, 26 and 29 nm.

In 1 M NaCl, the zeta potentials of the $T = 3$ and $T = 4$ capsids are relatively low, approximately −10 mV, and the 22 nm silica particles have a smaller zeta potential because their electrophoretic mobility, estimated from the dwell time in the nanopore, is lower than the HBV capsids. Moreover, the ratios of the pulse amplitudes of the $T = 3$ and $T = 4$ capsids measured in 0.4, 0.75, and 1 M NaCl are similar. Thus, it is appropriate to treat the 22 nm silica particles as nonconducting spheres for analysis of the RPS data.

With the standards outlined above, the $\Delta i/i$ values for the silica particles can be converted into diameters. The peak center for the silica NPs at $\Delta i/i = 0.178$ corresponds to a diameter of 22 nm, and the fwhm is 5 nm. There is also a small population for the silica NPs at $\Delta i/i$ of 0.258 which aligns well with the small peak at 14.5 MDa in the CD-MS mass distribution. While the average particle diameters obtained from TEM and RPS align, the RPS measurements indicated a higher concentration of larger particles than the CD-MS results.

**Analysis of 50 nm Silica NPs by RPS, EM, and CD-MS.** Silica NP sample 3, a 50 nm commercial sample, had a measured diameter of 51 ± 2 nm according to the certificate of analysis (based on 100 particles imaged with TEM). The measured CD-MS mass distribution is shown in Figure 3a. Only a single component is evident in the mass distribution. The average mass determined from a Gaussian fit to the measured distribution (dashed-dotted line in Figure 3a) is 82.5 MDa. The diameter distribution obtained from the CD-MS mass distribution with the density of fused silica (2.203 g/cm$^3$) is shown in Figure 3b. The distribution is centered at 49.2 nm and has a fwhm of 5.0 nm. As shown in Figure 3b, the diameter obtained from the TEM analysis (blue line) is slightly larger than the center of the distribution obtained from the CD-MS masses. This difference may indicate that the density of the 50 nm silica NPs is slightly less than the density of fused silica. A low density may result because the particles are porous.[17,19] Pores facilitate adsorption and controlled release of a cargo, and pores of various size regimes have been classified for silica NPs; macroporous particles have pores greater than 50 nm, mesoporous range from 2 to 50 nm, and microporous particles have pores less than 2 nm.

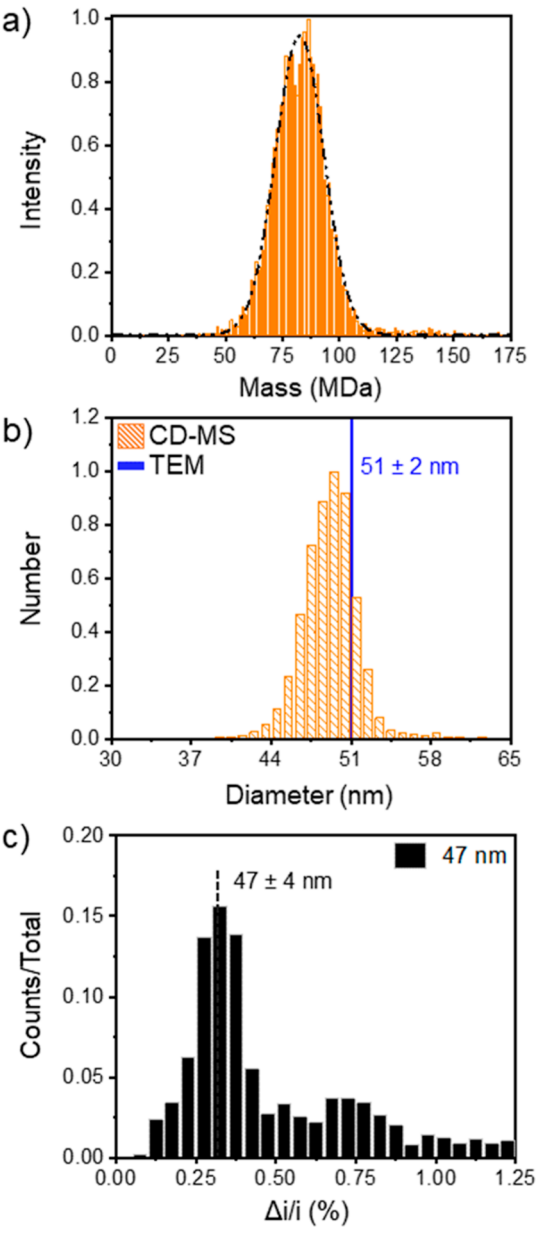


**Figure 3.** Analysis of 50 nm silica NPs commercial sample. (a) CD-MS mass distribution with a Gaussian fit (black dashed-dotted line). (b) Diameter distribution obtained from the mass distribution in (a) with the bulk density (see text). The blue line shows the average diameter obtained by TEM (from the certificate of analysis). (c) RPS distribution for the 50 nm silica NPs. Total counts were >6600 for CD-MS and >1100 for RPS.

Figure 3c shows the results for RPS analysis of the 50 nm silica NPs. 1144 particles were analyzed in around 30 min, and the figure shows the distribution of $\Delta i/i$ values. The peak in the distribution corresponds to a diameter of 47 nm. In addition, there is a broad tail extending to higher $\Delta i/i$ values. Thus, RPS measurements provide a diameter of 47 nm, CD-MS using the density of fused silica provides a diameter of 49


https://doi.org/10.1021/acs.analchem.4c02901
Anal. Chem. XXXX, XXX, XXX−XXX

nm, and TEM provides a diameter of 51 nm (according to the certificate of analysis). To shed light on these differences, we used SEM to determine the particle diameters. An average diameter of 46.3 nm was obtained with a distribution fwhm of 9.3 nm (see Figure S3). Several dumbbell-like particles are evident in the SEM images (see Figure S3a), raising the possibility that they are responsible for the high $\Delta i/i$ tail seen in the RPS measurements. However, that these structures are strongly bound seems unlikely because they are absent in the CD-MS measurements. They may be weakly bound aggregates that are present in solution and detected by RPS but do not survive the electrospray process and, hence, are not detected by CD-MS. The differences between the values obtained for the average particle diameters may partly reflect the different methods used to determine them. The values obtained from the CD-MS mass measurements depend on the particle density which may not be the same as the bulk value for fused silica (see below). The diameters obtained from EM (TEM and SEM) depend on accurate detection of NP edges. Also, the images are 2D projections and in 3D, the particles may not be perfectly spherical. For RPS, which is sensitive to particle volume, there is again the issue that the particle may not be spherical. Both RPS and SEM indicate that the average particle diameter is 46−47 nm. If we accept this value and combine it with the average mass determined by CD-MS, an average density of 2.53 g/cm$^3$ is obtained, which is outside the range previously reported for silica colloids and NPs (1.9−2.3 g/cm$^3$).[28,51] However, the density of quartz is 2.65 g/cm$^3$ so the high density obtained for the NPs with an average diameter of 47 nm could result because these silica NPs are more crystalline.

**Analysis of 40 nm Silica NPs by EM and CD-MS.** Sample 4, generated in-house by seed mediated growth, has three abundant peaks in the CD-MS mass distribution at 40.4 MDa (fwhm 8.6 MDa), 59.5 MDa (fwhm 11.4 MDa) and 75.1 MDa (fwhm 11.8 MDa) (see Figure 4a). The peak at 75.1 MDa is just under twice the mass of the 40.4 MDa species, so it is probably due to a dimer. The broad high mass tail extending past 100 MDa could also be due to aggregates. However, the peak at 59.5 MDa cannot be an aggregate of the peak at 40.4 MDa. Thus, the mass distribution for this sample appears to contain two components in addition to the higher mass aggregates.

A representative TEM image is shown in the inset in Figure 4a. An expanded view of this image and two other images are shown in Supporting Information. The blue histogram in Figure 4b shows the diameters determined from analysis of TEM images. The average diameter is 41.5 nm with a fwhm of 4.2 nm. There is a small component at a higher diameter (around 47.5 nm). The orange histogram in Figure 4b shows the size distribution obtained when the mass distribution in Figure 4a is converted into a diameter distribution with the density of fused silica (2.203 g/cm$^3$). Diameters corresponding to 38.8 nm (fwhm 2.8 nm) and 44.1 nm (fwhm 2.9 nm) are found along with larger diameters attributed to aggregates. The two lower mass components from the mass distribution have diameters (38.8 and 44.1 nm) that bracket the average diameter found from the TEM measurements (41.5 nm). Only a single size distribution was observed in the TEM studies, though we cannot rule out the possibility that there are two size distributions that overlap and cannot be resolved. The fwhm of the TEM size distribution is relatively small (4.2 nm),

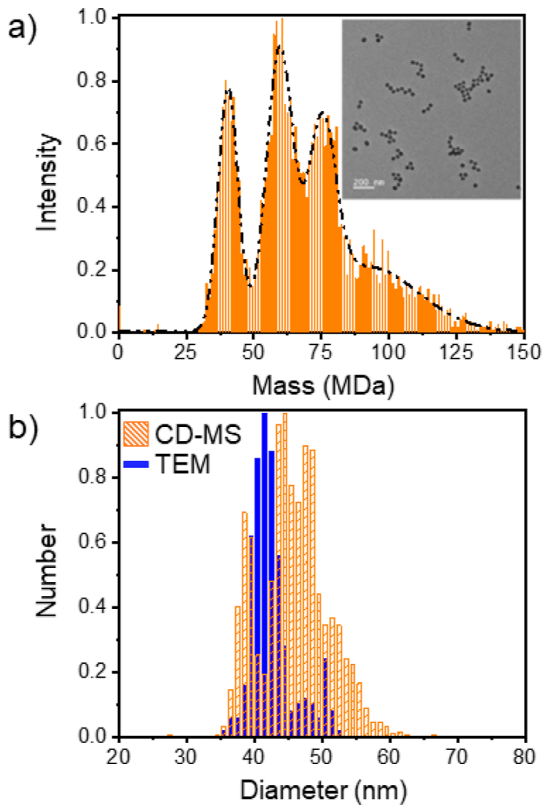


**Figure 4.** Analysis of 40 nm silica NPs generated by seed mediated growth. (a) CD-MS mass distribution with a sum of four Gaussians fit (black dashed-dotted line). (b) Diameter distribution obtained from the mass distribution in (a) with the density of fused silica (see text) (orange). The blue histogram shows the average diameter obtained by TEM. Total counts were >4000 for CD-MS and >250 for TEM.

so the two size distributions (if they exist) must have average sizes that are quite similar.

With the average TEM diameter of 41.5 nm, the peaks in the mass distribution at 40.4 MDa and 59.5 MDa lead to average densities of 1.67 and 2.46 g/cm$^3$, respectively. Both densities lie outside the range previously observed for silica colloids or NPs (1.9−2.3 g/cm$^3$).[28,51] The lower diameter particles in the TEM diameter distribution may make up the 40.4 MDa peak in the mass distribution, and the higher diameter particles may make up the 59.5 MDa peak in the mass distribution. This situation would raise the average density for the 40.4 MDa peak and lower the average density for the 59.5 MDa peak to the point where the average densities may lie inside the range previously observed for silica colloids and NPs. Regardless, these 40 nm silica particles clearly cannot be characterized by a single average density and the measurements indicate that there are two types of 40 nm silica NP with different densities. One plausible explanation for the different densities is that there porous and nonporous subpopulations. These results illustrate the importance of performing both CD-MS mass and size measurements to characterize NPs. In this case the TEM size distribution showed a single component while the CD-MS mass distribution showed two mass distributions with slightly different masses.

**Analysis of 70 nm Silica NPs by RPS, EM, and CD-MS.** Sample 5 was generated by seeded growth and had an average diameter of 71.6 nm with a fwhm of 5.3 nm from >250 particles analyzed from TEM images (Figure 5a,b). A similar


https://doi.org/10.1021/acs.analchem.4c02901
Anal. Chem. XXXX, XXX, XXX−XXX

average particle diameter was obtained from RPS measurement of >700 particles (see Figure 5c).

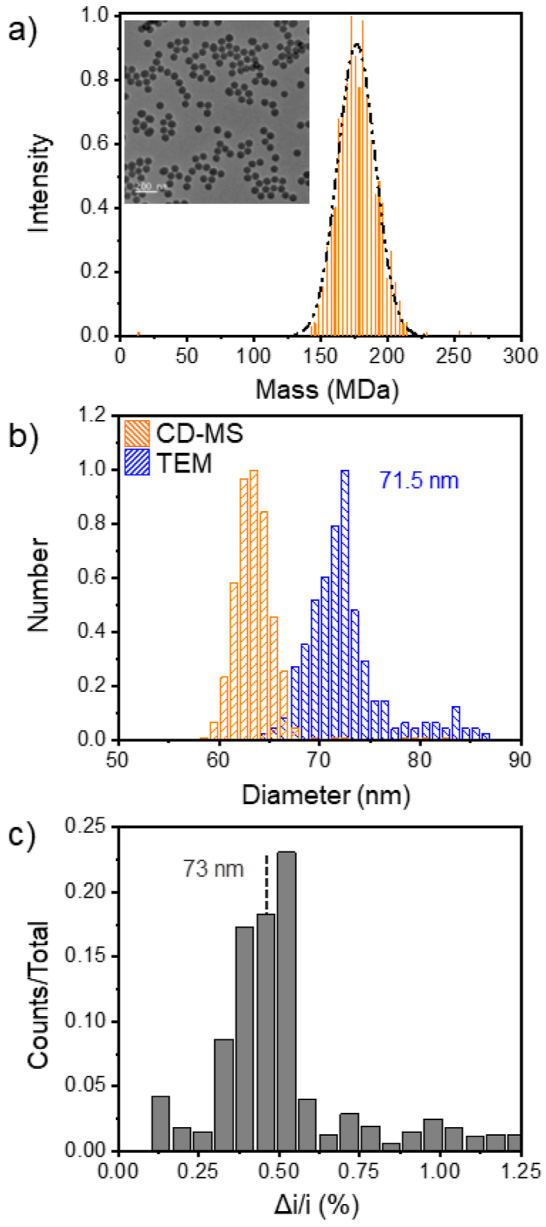


**Figure 5.** Analysis of 70 nm silica NPs prepared by seed mediated growth. (a) Mass distribution of the NPs. The dashed-dotted line shows a Gaussian fit to determine the average mass and fwhm. (b) Diameter distribution determined from the masses in (a) with the density of bulk fused silica (orange histogram). The blue histogram shows the diameter distribution obtained from analysis of the TEM images. The inset in (a) shows a representative TEM image used to determine the TEM diameter distribution. (c) RPS distribution of the 70 nm silica sample. Total counts were >700 for RPS and CD-MS and >250 for TEM.

The mass distribution for the 70 nm silica NPs is shown in Figure 5a. The distribution is close to Gaussian. It is centered on 176.5 MDa and has a fwhm of 33.1 MDa. The diameter distribution determined from the measured masses with the density of fused silica (2.203 g/cm$^3$) is shown in Figure 5b. The center of the distribution is at 63.36 nm, and the fwhm is 4.04 nm. Thus, the average diameter obtained from the masses with the density of fused silica is much smaller than the average diameters obtained from the TEM and RPS measurements. A silica NP with a diameter of 73 nm would have a mass of 274 MDa if it had the same density as fused silica (2.203 g/cm$^3$). The measured mass is 176.5 MDa, indicating that the average density of these silica NPs is 1.44 g/cm$^3$, 65% of the average value for fused silica, and outside the range previously observed for silica NPs (1.9−2.3 g/cm$^3$). Such a low density indicates that the particles are highly porous.

Table 2 shows a summary of the results for the five silica samples discussed above (three synthesized by seed mediated growth and two commercial products), and one additional sample (27 nm commercial) not discussed above. Diameters obtained by RPS and EM are given, along with the average masses and average charges determined by CD-MS. The average charge increases systematically with particle diameter and the particles synthesized in house and the commercial samples have similar size dependent behavior. Charge versus mass scatter plots for the NP samples discussed above are given in Figure S5.

**Table 2. Summary of RPS, EM, and CD-MS Measurements and Calculated Densities for Silica NP Samples**

| sample | source | average diameter (nm) | | average mass from CD-MS (MDa) | average charge from CD-MS (e) | density (g/cm$^3$) |
|---|---|---|---|---|---|---|
| | | EM | RPS | | | |
| 1 | synthesized in-house | 19.4 | | 5.1 | 86 | 2.20 |
| 2 | commercial | 22.2[a] | 22 | 7.5 | 101 | 2.20 |
| 3 | commercial | 46.3/51[a] | 47 | 82.5 | 417 | 2.53 |
| 4a | synthesized in-house | 41.5 | | 40.4 | 299 | 1.67 |
| 4b | synthesized in-house | 41.5 | | 59.5 | 373 | 2.46 |
| 5 | synthesized in-house | 71.5 | 73 | 177.0 | 688 | 1.44 |
| ND[b] | commercial | 27[a] | | 14.7 | 156 | 2.37 |

[a]Determined by manufacturer. [b]Not discussed above.

The main limitation to the accuracy of the density measurements determined using the approach described here is the particle diameter, not least because it enters into the equation for the density as the cube. The mass distribution measured by CD-MS is accurate and unambiguous. However, the diameter determined from EM is subject to uncertainty because the particles are not perfectly spherical and because of the difficulty in defining the particle edges. RPS, which provides a volume-based measurement, should, in principle, provide a better estimate of the particle diameter.

For samples 1 and 2, 19 nm synthesized and 22 nm commercial particles, respectively, the densities are close to the density of fused silica. For the 50 nm commercial product, RPS and SEM provided diameters of 46/47 nm, considerably smaller than the 51 nm value determined by the manufacturer using limited TEM analysis. Using the smaller diameter and the measured mass led to a density of 2.53 g/cm$^3$, which is outside the 1.9−2.3 g/cm$^3$ range previously found for silica colloids and NPs.[28,51] Sample 4, synthesized by seed mediated growth, was unusual in having two primary mass peaks, but only a single prominent peak in the TEM diameter distribution. These observations suggest that sample 4 contains


https://doi.org/10.1021/acs.analchem.4c02901
Anal. Chem. XXXX, XXX, XXX−XXX

two types of silica NPs with different densities. One plausible explanation for the different densities is that there are porous and nonporous subpopulations. Finally, sample 5, generated by seed mediated growth had an average diameter of 72 nm by TEM and 73 nm by RPS. The mass distribution showed a single prominent peak at 177 MDa. The average mass and average diameter led to a density of 1.44 g/cm$^3$, which is outside the 1.9−2.3 g/cm$^3$ range normally found for silica colloids and NPs.[28,51] The low density suggests that these NPs contain pores or voids.

While sample 4 contains two types of silica NPs with different densities, for the other samples investigated here a single density is deduced from the average mass and average volume obtained from different experiments. However, even for samples where a single average density is deduced, it is unlikely that the particles all have the same densities. The particles in all of the samples probably have a distribution of densities, just as they have a distribution of masses and volumes. The density distribution would be revealed by single particle measurements of mass and volume for individual particles. Such a correlated measurement is not possible using the approach described here.

## CONCLUSIONS

NP size distributions are usually characterized by TEM. In this work, in addition to EM based methods, we have also employed RPS, a technique that measures particle volume, and CD-MS, a method that determines the NP mass distributions. Most of the samples examined here showed a single prominent peak in the diameter distribution, and the average diameters obtained from EM and RPS were similar. Sample 3 was the exception. In this case, the average particle size determined by the manufacturer using TEM was significantly larger than the average diameter determined with RPS and SEM.

By combining the average diameter with the average mass, the NP density can be determined. For the smallest silica NPs (samples 1 and 2 at 19 and 22 nm, respectively) the densities were in close agreement with the density of fused silica (2.203 g/cm$^3$). For larger particles we found examples where the densities were smaller and larger than 2.203 g/cm$^3$ and fall outside the range of densities usually found for silica colloids and NPs (1.9−2.3 g/cm$^3$).[49,50] For one sample (sample 4) the diameter distribution showed a single component, and the mass distribution showed two peaks. These results suggest that the sample contained two populations of silica NPs with different densities. Taken together, the results show that much more in-depth information can be obtained from a combination of EM, RPS, and CD-MS than can be obtained from any single method alone.

Density is one of the most important physical properties for atmospheric aerosols, particles with sizes between several nanometers and microns, because it influences their transport properties and radiative forcing. Particle density is also needed to convert ambient particle number densities to mass concentrations that are related to visibility and air quality. Because of the difficulty of measuring the density for aspherical aerosol particles, measurement of the effective density has been adopted as an alternative. A variety of techniques have been developed to measure the effective density.[60] For example, the combination of a differential mobility analyzer, centrifugal particle mass analyzer, and condensation particle counter has been frequently used to analyze aerosols emitted from vehicles and biomass combustion. The use of mobility-based methods to determine particle size (the orientationally averaged collision integral) could be combined with CD-MS measurement of the mass. Furthermore, this combination could be performed in a correlated manner where size and mass are measured for individual particles, so that a density distribution could be determined.

## ASSOCIATED CONTENT

### Supporting Information

The Supporting Information is available free of charge at https://pubs.acs.org/doi/10.1021/acs.analchem.4c02901.

Design and operation of RPS device, figure showing sonication reduces aggregation of silica NPs, size distribution of 50 nm NPs by SEM, TEM images of 40 nm silica NPs, and CD-MS charge versus mass scatter plots for all samples (PDF)

## AUTHOR INFORMATION


### Corresponding Authors

**Stephen C. Jacobson** − *Department of Chemistry, Indiana University, Bloomington, Indiana 47405, United States;* orcid.org/0000-0003-2415-041X; Email: jacobson@iu.edu

**Martin F. Jarrold** − *Department of Chemistry, Indiana University, Bloomington, Indiana 47405, United States;* orcid.org/0000-0001-7084-176X; Email: mfj@iu.edu

### Authors

**Lohra M. Miller** − *Department of Chemistry, Indiana University, Bloomington, Indiana 47405, United States*

**Tanner W. Young** − *Department of Chemistry, Indiana University, Bloomington, Indiana 47405, United States*

**Yi Wang** − *Department of Chemistry, Indiana University, Bloomington, Indiana 47405, United States;* orcid.org/0000-0003-2882-8777

**Benjamin E. Draper** − *Department of Chemistry, Indiana University, Bloomington, Indiana 47405, United States;* orcid.org/0000-0002-9727-2509

**Xingchen Ye** − *Department of Chemistry, Indiana University, Bloomington, Indiana 47405, United States;* orcid.org/0000-0001-6851-2721

Complete contact information is available at: https://pubs.acs.org/10.1021/acs.analchem.4c02901

### Author Contributions

†L.M.M. and T.W.Y contributed equally.


### Notes

The authors declare the following competing financial interest(s): Two of the authors (BED and MFJ) are shareholders in Megadalton Solutions, a company that is engaged in commercializing CD-MS. MFJ is a consultant for Waters.

## ACKNOWLEDGMENTS

This work was supported in part by NIH R35 GM141922 and NSF CHE-0923064 for T.W.Y. and S.C.J. Y.W. and X.Y. acknowledge financial support from the National Science Foundation Center for Single-Entity Nanochemistry and Nanocrystal Design (CHE-2221062). The authors thank the Indiana University Nanoscale Characterization Facility and Electron Microscopy Center for the use of their instruments. The authors thank Quintin J. Brown, Ethan D. Call, Michael P.

Kappler and Sheng-Yuan Huang for supporting data for resistive-pulse measurements with HBV capsids.

## REFERENCES

(1) Janjua, T. I.; Cao, Y.; Yu, C.; Popat, A. *Nat. Rev. Mater.* **2021**, *6*, 1072−1074.
(2) Dagan, N.; Barda, N.; Kepten, E.; Miron, O.; Perchik, S.; Katz, M. A.; Hernán, M. A.; Lipsitch, M.; Reis, B.; Balicer, R. D. *N. Engl. J. Med.* **2021**, *384*, 1412−1423.
(3) Sung, Y. K.; Kim, S. W. *Biomater. Res.* **2020**, *24*, 12.
(4) Farokhzad, O. C.; Langer, R. *Adv. Drug Delivery Rev.* **2006**, *58*, 1456−1459.
(5) Langer, R. *Nature* **1998**, *392* (6679 Suppl), 5−10.
(6) Cannio, M.; Bellucci, D.; Roether, J. A.; Boccaccini, D. N.; Cannillo, V. *Materials* **2021**, *14*, 5440.
(7) Batz, N. G.; Mellors, J. S.; Alarie, J. P.; Ramsey, J. M. *Anal. Chem.* **2014**, *86*, 3493−3500.
(8) Huhn, C.; Ramautar, R.; Wuhrer, M.; Somsen, G. W. *Anal. Bioanal. Chem.* **2010**, *396*, 297−314.
(9) Vallet-Regi, M.; Ramila, A.; del Real, R. P.; Perez-Pariente, J. *Chem. Mater.* **2001**, *13*, 308−311.
(10) Doadrio, J. C.; Sousa, E. M. B.; Izquierdo-Barba, I.; Doadrio, A. L.; Perez-Pariente, J.; Vallet-Regi, M. *J. Mater. Chem.* **2006**, *16*, 462−466.
(11) Mehmood, A.; Ghafar, H.; Yaqoob, S.; Gohar, U. F.; Ahmad, B. *J. Dev. Drugs* **2017**, *06*, 174.
(12) Radu, D. R.; Lai, C.-Y.; Jeftinija, K.; Rowe, E. W.; Jeftinija, S.; Lin, V. S.-Y. *J. Am. Chem. Soc.* **2004**, *126*, 13216−13217.
(13) Slowing, I.; Trewyn, B. G.; Lin, V. S.-Y. *J. Am. Chem. Soc.* **2006**, *128*, 14792−14793.
(14) Chen, J.-F.; Ding, H.-M.; Wang, J.-X.; Shao, L. *Biomaterials* **2004**, *25*, 723−727.
(15) Song, Y.; Du, D.; Li, L.; Xu, J.; Dutta, P.; Lin, Y. *ACS Appl. Mater. Interfaces* **2017**, *9*, 20410−20416.
(16) de Souza e Silva, J. M.; Hanchuk, T. D. M.; Santos, M. I.; Kobarg, J.; Bajgelman, M. C.; Cardoso, M. B. *ACS Appl. Mater. Interfaces* **2016**, *8*, 16564−16572.
(17) Kresge, C. T.; Leonowicz, M. E.; Roth, W. J.; Vartuli, J. C.; Beck, J. S. *Nature* **1992**, *359*, 710−712.
(18) Ying, J. Y.; Mehnert, C. P.; Wong, M. S. *Angew. Chem., Int. Ed.* **1999**, *38*, 56−77.
(19) Huh, S.; Wiench, J. W.; Yoo, J.-C.; Pruski, M.; Lin, V. S.-Y. *Chem. Mater.* **2003**, *15*, 4247−4256.
(20) Trewyn, B. G.; Whitman, C. M.; Lin, V. S.-Y. *Nano Lett.* **2004**, *4*, 2139−2143.
(21) Suzuki, K.; Ikari, K.; Imai, H. *J. Am. Chem. Soc.* **2004**, *126*, 462−463.
(22) Ying, J. Y. *Chem. Eng. Sci.* **2006**, *61*, 1540−1548.
(23) Fakoya, M. F.; Shah, S. N. *Petroleum* **2017**, *3*, 391−405.
(24) Lim, J.; Yeap, S. P.; Che, H. X.; Low, S. C. *Nanoscale Res. Lett.* **2013**, *8*, 381.
(25) Wang, Y.; Chen, J.; Zhu, C.; Zhu, B.; Jeong, S.; Yi, Y.; Liu, Y.; Fiadorwu, J.; He, P.; Ye, X. *Nano Lett.* **2021**, *21*, 5053−5059.
(26) Ye, X.; Zhu, C.; Ercius, P.; Raja, S. N.; He, B.; Jones, M. R.; Hauwiller, M. R.; Liu, Y.; Xu, T.; Alivisatos, A. P. *Nat. Commun.* **2015**, *6*, 10052.
(27) Anderson, W.; Kozak, D.; Coleman, V. A.; Jämting, Å. K.; Trau, M. *J. Colloid Interface Sci.* **2013**, *405*, 322−330.
(28) Kimoto, S.; Dick, W. D.; Hunt, B.; Szymanski, W. W.; McMurry, P. H.; Roberts, D. L.; Pui, D. Y. H. *Aerosol Sci. Technol.* **2017**, *51*, 936−945.
(29) Coulter, W. H. Means for Counting Particles Suspended in a Fluid. U.S. Patent 2,656,508 A, 1953.
(30) DeBlois, R. W.; Bean, C. P. *Rev. Sci. Instrum.* **1970**, *41*, 909−916.
(31) Young, T. W.; Kappler, M. P.; Hockaden, N. M.; Carpenter, R. L.; Jacobson, S. C. *Anal. Chem.* **2023**, *95*, 16710−16716.
(32) Harms, Z. D.; Mogensen, K. B.; Nunes, P. S.; Zhou, K.; Hildenbrand, B. W.; Mitra, I.; Tan, Z.; Zlotnick, A.; Kutter, J. P.; Jacobson, S. C. *Anal. Chem.* **2011**, *83*, 9573−9578.
(33) Harms, Z. D.; Selzer, L.; Zlotnick, A.; Jacobson, S. C. *ACS Nano* **2015**, *9*, 9087−9096.
(34) Kondylis, P.; Zhou, J.; Harms, Z. D.; Kneller, A. R.; Lee, L. S.; Zlotnick, A.; Jacobson, S. C. *Anal. Chem.* **2017**, *89*, 4855−4862.
(35) Doussineau, T.; Desert, A.; Lambert, O.; Taveau, J.-C.; Lansalot, M.; Dugourd, P.; Bourgeat-Lami, E.; Ravaine, S.; Duguet, E.; Antoine, R. *J. Phys. Chem. C* **2015**, *119*, 10844−10849.
(36) Draper, B. E.; Anthony, S. N.; Jarrold, M. F. *J. Am. Soc. Mass Spectrom.* **2018**, *29*, 2160−2172.
(37) Harper, C. C.; Miller, Z. M.; McPartlan, M. S.; Jordan, J. S.; Pedder, R. E.; Williams, E. R. *ACS Nano* **2023**, *17*, 7765−7774.
(38) Shelton, H.; Hendricks, C. D.; Wuerker, R. F. *J. Appl. Phys.* **1960**, *31*, 1243−1246.
(39) Fuerstenau, S. D.; Benner, W. H. *Rapid Commun. Mass Spectrom.* **1995**, *9*, 1528−1538.
(40) Fuerstenau, S. D.; Benner, W. H.; Thomas, J. J.; Brugidou, C.; Bothner, B.; Siuzdak, G. *Angew. Chem., Int. Ed.* **2001**, *40*, 541−544.
(41) Benner, W. H. *Anal. Chem.* **1997**, *69*, 4162−4168.
(42) Contino, N. C.; Jarrold, M. F. *Int. J. Mass Spectrom.* **2013**, *345*−*347*, 153−159.
(43) Contino, N. C.; Pierson, E. E.; Keifer, D. Z.; Jarrold, M. F. *J. Am. Soc. Mass Spectrom.* **2013**, *24*, 101−108.
(44) Pierson, E. E.; Keifer, D. Z.; Contino, N. C.; Jarrold, M. F. *Int. J. Mass Spectrom.* **2013**, *337*, 50−56.
(45) Pierson, E. E.; Contino, N. C.; Keifer, D. Z.; Jarrold, M. F. *J. Am. Soc. Mass Spectrom.* **2015**, *26*, 1213−1220.
(46) Keifer, D. Z.; Shinholt, D. L.; Jarrold, M. F. *Anal. Chem.* **2015**, *87*, 10330−10337.
(47) Keifer, D. Z.; Pierson, E. E.; Jarrold, M. F. *Analyst* **2017**, *142*, 1654−1671.
(48) Jarrold, M. F. *Chem. Rev.* **2022**, *122*, 7415−7441.
(49) Hanozin, E.; Harper, C. C.; McPartlan, M. S.; Williams, E. R. *ACS Cent. Sci.* **2023**, *9*, 1611−1622.
(50) Jarrold, M. F. *J. Am. Chem. Soc.* **2024**, *146*, 5749−5758.
(51) Watanabe, R.; Yokoi, T.; Kobayashi, E.; Otsuka, Y.; Shimojima, A.; Okubo, T.; Tatsumi, T. *J. Colloid Interface Sci.* **2011**, *360*, 1−7.
(52) Harms, Z. D.; Haywood, D. G.; Kneller, A. R.; Selzer, L.; Zlotnick, A.; Jacobson, S. C. *Anal. Chem.* **2015**, *87*, 699−705.
(53) Raillon, C.; Granjon, P.; Graf, M.; Steinbock, L. J.; Radenovic, A. *Nanoscale* **2012**, *4*, 4916−4924.
(54) Draper, B. E.; Jarrold, M. F. *J. Am. Soc. Mass Spectrom.* **2019**, *30*, 898−904.
(55) Schmidt, H. T.; Cederquist, H.; Jensen, J.; Fardi, A. *Nucl. Instrum. Methods Phys. Res., Sect. B* **2001**, *173*, 523−527.
(56) Reitenbach, D. W.; Botamanenko, D. Y.; Miller, L. M.; Jarrold, M. F. *Anal. Chem.* **2024**, accepted.
(57) Parikh, R. A.; Draper, B. E.; Jarrold, M. F. *Anal. Chem.* **2024**, *96*, 3062−3069.
(58) Crowther, R. A.; Kiselev, N. A.; Böttcher, B.; Berriman, J. A.; Borisova, G. P.; Ose, V.; Pumpens, P. *Cell* **1994**, *77*, 943−950.
(59) Wingfield, P. T.; Stahl, S. J.; Williams, R. W.; Steven, A. C. *Biochemistry* **1995**, *34*, 4919−4932.
(60) Peng, L.; Li, Z.; Zhang, G.; Bi, X.; Hu, W.; Tang, M.; Wang, X.; Peng, P.; Sheng, G. *Sci. Total Environ.* **2021**, *778*, 146248.


https://doi.org/10.1021/acs.analchem.4c02901
*Anal. Chem.* XXXX, XXX, XXX−XXX